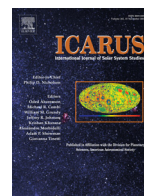




ELSEVIER

Contents lists available at ScienceDirect

Icarus

journal homepage: www.elsevier.com/locate/icarus

Decadal timescale variability of the Enceladus plumes inferred from Cassini images

Andrew P. Ingersoll*, Shawn P. Ewald

Division of Geological and Planetary Sciences, California Institute of Technology, Pasadena, CA 91125, USA

ARTICLE INFO

Article history:

Received 30 January 2016

Revised 8 September 2016

Accepted 12 September 2016

Available online xxx

Keywords:

Enceladus

Saturn satellites

Satellites

Atmospheres

ABSTRACT

The brightness of the Enceladus plumes varies with position in the satellite's eccentric orbit, with altitude above the surface, and with time from one year to the next. Hedman et al. (2013, hereinafter H13) were the first to report these variations. They used data from Cassini's Visible and Infrared Mapping Spectrometer (VIMS). Here we present brightness observations from Cassini's Imaging Science Subsystem (ISS), which has 40 times higher spatial resolution than VIMS. Our unit of measure is slab density, the total mass of particles in a horizontal slab per unit thickness of the slab. Using slab density is one approach to correcting for the variation of brightness with wavelength and scattering angle. Approaches differ mainly by a multiplicative scaling factor that depends on particle density, which is uncertain. All approaches lead to the same qualitative conclusions and agree with the conclusions from VIMS. We summarize our conclusions as follows: At all altitudes between 50 and 200 km, the corrected brightness is 4–5 times greater when Enceladus is farther from Saturn (near apocenter) than when it is closer (near pericenter). A secondary maximum occurs after pericenter and before apocenter. Corrected brightness vs. altitude is best described as a power law whose negative exponent is greatest in magnitude at apocenter, indicating a slower launch speed for the particles at apocenter than at other points in the orbit. Corrected brightness decreased by roughly a factor of two during much of the period 2005–2015. The last is our principal result, and we offer three hypotheses to explain it. One is a long-period tide—the decreasing phase of an 11-year cycle in orbital eccentricity; another is buildup of ice at the throats of the vents; and the third is seasonal change—the end of summer at the south pole.

© 2016 Elsevier Inc. All rights reserved.

1. Introduction

Properties of the Enceladus plumes tell us about subsurface conditions. Salt dissolved in the icy particles suggests that the main plume source is a saltwater solution in contact with warm rock, but the presence of salt-free particles suggests other sources as well (Postberg et al., 2009, 2011). Salinity greater than 16 g kg^{-1} is necessary to keep the liquid surface from freezing (Ingersoll and Nakajima, 2016), and that value is consistent with the observations (Postberg et al., 2009). The rate of boiling is controlled by friction of the gas with the walls of the crack (Nakajima and Ingersoll, 2016), and could be quite slow. At least 90% of the energy emerges as infrared radiation from the icy surface (Howett et al., 2011; Spencer et al., 2013) and only ~10% emerges as latent heat associated with the vapor (Hansen et al., 2006, 2008, 2011). Either energy is carried by the vapor, which condenses near the tops of the vents (Ingersoll and Pankine, 2010), or by the liquid,

which circulates up and down in the vents (Matson et al., 2012; Ingersoll and Nakajima, 2016; Kite and Rubin, 2016). In both cases, the heat is conducted through the ice at the surface and radiated to space. The particle size distribution and ice to vapor mass ratio reveal how the particles are forming, but estimates of the latter are still uncertain (Porco et al., 2006; Ingersoll and Ewald, 2011, hereinafter IE11; Gao et al., 2016). The focus of the present paper is on the temporal variability and height distribution of plume material, which provide information about the geometry of the vents and the opening and closing of the fissures (Hurford et al., 2007; Schmidt et al., 2008; Hedman et al., 2009; H13; Nimmo et al., 2014, hereinafter N14; Porco et al., 2014).

Using data from the Cassini Visible and Infrared Mapping Spectrometer (VIMS) instrument, H13 found that plume brightness varies with orbital phase. The brightness values near apocenter are 4–5 times the values near pericenter. They point out that geophysical models (Hurford et al., 2007) predict the fissures should be under tension at apocenter and therefore should be wider open compared to other times, which is consistent with the observations. H13 made two other observations. One is that the data taken in 2005 yielded brightness levels that are 50% higher than data

* Corresponding author. Fax: 01 626 585 1917.

E-mail addresses: api@gps.caltech.edu (A.P. Ingersoll), spe@gps.caltech.edu (S.P. Ewald).

<http://dx.doi.org/10.1016/j.icarus.2016.09.018>

0019-1035/© 2016 Elsevier Inc. All rights reserved.

taken in 2009–2012. This would indicate some long-term temporal change in addition to the change in phase with the 1.37-day orbit cycle. The other observation is that brightness seems to fall off with altitude faster at apocenter than at pericenter. This would indicate that the particles are launched with a larger maximum speed when Enceladus is near to its orbital pericenter than when it is near apocenter.

Here we report on an analysis that uses the narrow angle camera (NAC) of the Imaging Science Subsystem (ISS) instrument (Porco et al., 2004; West et al., 2010). The NAC has a resolution of 6 μ rad per pixel. For a typical NAC image used in this study the resolution is 1 km, and for a typical VIMS image the resolution is 40 km. For measuring the geometry of the plumes, the NAC has several advantages. First, the high resolution perpendicular to the plume axis allows one to accurately separate the E ring background from the wings of the plumes. Second, one can determine the vertical profile of brightness at high resolution. Third, one can measure the brightness of the plume at low altitudes without interference from the bright crescent of Enceladus. Fourth, the NAC can take images at a relatively high rate, which improves the time coverage.

N14 also used NAC images. They focused exclusively on the orbital cycle and reported that maximum brightness occurred at a mean anomaly (MA) of $\sim 210^\circ$. MA is the time measured from pericenter, divided by the orbit period and multiplied by 360° . They attributed this phase lag as due to a warm ice shell that flows viscously in response to the tides. The time when the fissures are most likely to be open is therefore shifted later from $MA = 180^\circ$, which is the predicted value for a purely elastic shell (Hurford et al., 2007). The present paper uses a much larger data set than that used by N14. We find a more complicated behavior, including a secondary maximum during the quarter-cycle immediately after pericenter. Complications are expected too, since plume activity might depend both on shear stress and normal stress in the moon's crust, as well as on the orientation of individual cracks (Hurford et al., 2007; Smith-Konter and Pappalardo, 2008; Hurford et al., 2012).

In the data analysis, the two main difficulties are subtraction of light from the E ring background and conversion of observed brightness to column mass density. Section 2 describes the methods we used to surmount these difficulties and the tests we used to estimate the remaining errors. We compare our results to those of N14 and H13 and find a small systematic bias, which we attribute to different methods of background subtraction. The casual reader, or one interested mainly in the results, should treat Section 2 as an appendix, useful for later reference. Section 3.1 presents our principal result, which is that the overall plume brightness decreased by a factor of 2 over the past decade. In Section 3.2 we present further tests and figures to back up this claim. Section 3.3 is about phase lags and perhaps a secondary maximum. Section 3.4 presents our results concerning the vertical profiles of plume brightness. Section 4 presents a discussion of possible mechanisms that might cause plume brightness to decrease over the past decade. The Supplementary Online Material (SOM) contains additional images, tables of NAIF/SPICE kernels, constants for conversion from brightness to column mass density, and information about each of the images used in our data analysis.

2. Data analysis

The routine steps of data analysis, including selection of images, calibration, and determination of camera pointing, are given in the SOM. Table S1 contains a list of NAIF/SPICE kernels used in the analysis. Table S2 lists all the ISS images used in the analysis. Table S3 lists images of Enceladus with scattering angles less

than 40° that were *not* used in the analysis and the reasons for not using them. Examples include: electronic noise, stray light, camera motion, saturated pixels, and planet or rings in the background. We used only images for which the limb of Enceladus was visible and suitable for navigation. Here we focus on the steps that are particular to the Enceladus data: subtracting the E ring background, comparing with observations of H13 and N14, and converting observed brightness into column mass density.

2.1. Background subtraction and equivalent width

We want to know slab density—the mass of particles per unit thickness of a horizontal plane above the south pole and how it varies with altitude and time. What we measure is equivalent width, $EW = \int I/F dx$, which is computed by summing the I/F values in a line of pixels perpendicular to the Enceladus rotation axis and then multiplying by the projected pixel size, perpendicular to the line of sight at the distance to the Enceladus center, in km. Thus x becomes distance along the line of pixels, and EW is given in units of km. The plumes are optically thin, so EW captures all the light from the particles in a horizontal plane one projected pixel thick at the altitude of the line. Since Enceladus and its plumes are silhouetted against the E ring, light from the background has to be subtracted off before doing the integral. The analysis in Sections 2.1–2.3 is for EW at an altitude of 100 km. In Section 2.4 we discuss the conversion to slab density.

The above plan requires some approximations, but they are small. First, the spacecraft was not always in the equatorial plane of Enceladus when observations were taken. In the years before 2008 the spacecraft latitude θ_s ranged up to 15° , which means the plane was tilted relative to the polar axis—it is not strictly horizontal, and the optical path through the plume is increased by a factor $1/\mu = 1/\cos\theta_s = 1.035$ for $\theta_s = 15^\circ$. In this paper we ignore this deviation from unity. We also ignore the fact that the pole could be as much as $(1/\mu - 1)R = 8.8$ km below the horizon as seen from the spacecraft, where R is the moon's radius. We define altitude relative to the limb, which means we are ignoring this small altitude uncertainty. In the later years, θ_s was never more than 5° , so the pole was no more than 0.95 km below the horizon and the uncertainty is even less. Finally, the camera was not always lined up parallel to the polar axis, so we had to numerically rotate the image so that the moon's rotation axis was perpendicular to the line of pixels.

Background subtraction involves taking the pixels outside the plume on both sides, on the left from $-x_2 < x < -x_1$ and on the right from $x_1 < x < x_2$, and then fitting a function to them. Here $x = 0$ is the moon's spin axis; $\pm x_1$ is the assumed edge of the plume; $\pm x_2$ is outside $\pm x_1$, i.e., $|x_2| > |x_1| > 0$, and is limited only by the edge of the image. With a low-order polynomial for the background function, EW is the measured intensity minus the inferred background intensity, their difference integrated from $-x_1$ to x_1 . We tried this method with a quadratic function for the background, experimenting with different values of x_1 and x_2 and images of different projected pixel sizes, but there were problems. First, decreasing the values of x_1 and x_2 caused the negative curvature $-d^2(I/F)/dx^2$ to increase and the $EW = \int I/F dx$ to decrease, often by a factor of 2, even though curvature and EW are properties of the image and should not depend on x_1 and x_2 . Further, the negative curvature was always an order of magnitude greater than what we obtained for the E ring when Enceladus was not in the image (Figs. 3–5 of IE11) or when we were using a line of pixels to the north of Enceladus, far from the plume. In other words, the quadratic was consistently overestimating the negative curvature of the background, especially when x_1 and x_2 were small, e.g., 200 and 400 km, respectively. The actual brightness

Download English Version:

<https://daneshyari.com/en/article/5487417>

Download Persian Version:

<https://daneshyari.com/article/5487417>

[Daneshyari.com](https://daneshyari.com)